Appendix 1

Detailed method for automated image cropping

The UTE images were cropped to a 128×128 pixel (64×64 mm) region centered on the L5 vertebral body prior to CEP segmentation. This cropping process was automated to facilitate objective, repeatable, and rapid isolation of a region encompassing the L4-L5 and L5-S1 CEPs. To do this, a previously developed neural network (25) was used to first segment the lumbar vertebral bodies from the CSE images (Figure S1). The centroid of the L5 vertebra was computed based on these vertebral segmentations and then mapped from CSE space to UTE space (IDL 8.8) utilizing information embedded in the DICOM metadata:

$$\begin{bmatrix} i \\ j \\ 0 \\ 1 \end{bmatrix}_{UTE} = \begin{bmatrix} X_x\Delta i & Y_x\Delta j & 0 & S_x \\ X_y\Delta i & Y_y\Delta j & 0 & S_y \\ X_z\Delta i & Y_z\Delta j & 0 & S_z \\ 0 & 0 & 0 & 1 \end{bmatrix}^{-1}_{UTE} \left(\begin{bmatrix} X_x\Delta i & Y_x\Delta j & 0 & S_x \\ X_y\Delta i & Y_y\Delta j & 0 & S_y \\ X_z\Delta i & Y_z\Delta j & 0 & S_z \\ 0 & 0 & 0 & 1 \end{bmatrix}_{CSE} \begin{bmatrix} i \\ j \\ 0 \\ 1 \end{bmatrix}_{CSE} \right)$$

where i, j index the row, column pixel location, respectively; Δi, Δj represent the row, column pixel spacing (mm); X_{xyz} and Y_{xyz} represent the coordinate-system directional cosines, defined in the DICOM standard as Image Orientation (Patient) (0020, 0037); and S_{xyz} represents the reference coordinate system origin, defined in the DICOM standard as Image Position (Patient) (0020, 0032).

Appendix 2

Second scanner analysis

To assess the generalizability of the models to images collected at other sites, we acquired UTE and CSE MRI data at 3.0-Tesla from five patients with cLBP [mean ± SD age =57.8±14.0 years, numeric rating scale (NRS) =5.6±1.9, PEG score =6.1±3.0, one female and four males] imaged at a separate academic research hospital. Subjects were imaged with 3.0-Tesla MRI (Discovery MR750 scanner, GE Healthcare) using an 8-channel phased-array spine coil to collect sagittal acquisitions of the lumbar spine from a 3D UTE cones sequence and a CSE water-fat sequence. The UTE echo times were 0.032, 5.0, 10.2, 15.2, 20.2, and 25.2 ms. All other imaging parameters were identical to those described previously.

Additionally, we imaged five phantoms comprised of varying agarose concentrations (2%, 4%, 6%, 8%, 10% agarose diluted in de-ionized water by weight; type VII agarose, Sigma #A0701) at two timepoints (five months apart) using the primary scanner and at a single timepoint using the secondary scanner. The goal of this phantom analysis was to assess whether similar UTE sequences applied across different scanners can yield similar T2* relaxation-time values for biochemically equivalent specimens. Mean T2* values in each of the five phantoms from each scan were computed using a 16×16×24 mm cuboidal ROI placed in the phantom's center. We used linear regression to assess whether the relationship between agarose concentration and 1/T2* value differed within or between scanners (intra- and inter-scanner variability, respectively).

Results

In the five patients imaged, three levels from two patients were excluded due to endplate damage precluding CEP delineation (Figure S2). CEP CNR and SNR values in the second scanner were approximately 1.5- and 2-fold higher, respectively, than those in the primary scanner. SNR values were on average 21.2±3.4 (range, 15.3–27.6). CNR values between the CEP and adjacent vertebra (7.4±1.8, 4.0–10.1) were greater than those between the CEP and adjacent disc (3.3±1.0, 1.9–5.9). Compared to images collected using the primary scanner, the neural networks demonstrated similar levels of segmentation performance when applied to images collected using the second scanner: the sensitivity ranged from 0.733–0.853, specificity from 0.996–0.998, Dice coefficient from 0.754–0.828, and PR-AUC from 0.503–0.630. There was a relatively narrow range

https://dx.doi.org/10.21037/qims-22-729

of CEP T2* values (9.3–17.5 ms) in these patients. Model-predicted segmentations yielded unbiased estimates of mean T2* values and of principal CEP angle (Figure S3). Mean (95% CI) bias in T2* estimates was 0.03 ms (-0.97–1.02); mean bias in the angle estimates was 1.41° (–0.10, 2.91). There were high levels of overall agreement: 94% (16/17) of predicted CEP T2* values were within ±4.0 ms, and 88% (15/17) of predicted angles were within ±5° of the respective values computed manually.

For all agarose concentrations, T2* values were similar between phantoms imaged at both sites, and at the two timepoints imaged at the primary site (Figure S4). Mean phantom 1/T2* value was significantly associated with agarose concentration (R^2 =0.98, P<0.0001), and the relationship between agarose concentration and 1/T2* value was not different between or within scanners (P=0.75 for an interaction between agarose concentration and acquisition group). These data indicate that similar UTE sequences applied across scanners can yield similar T2* relaxation time values for biochemically equivalent specimens.

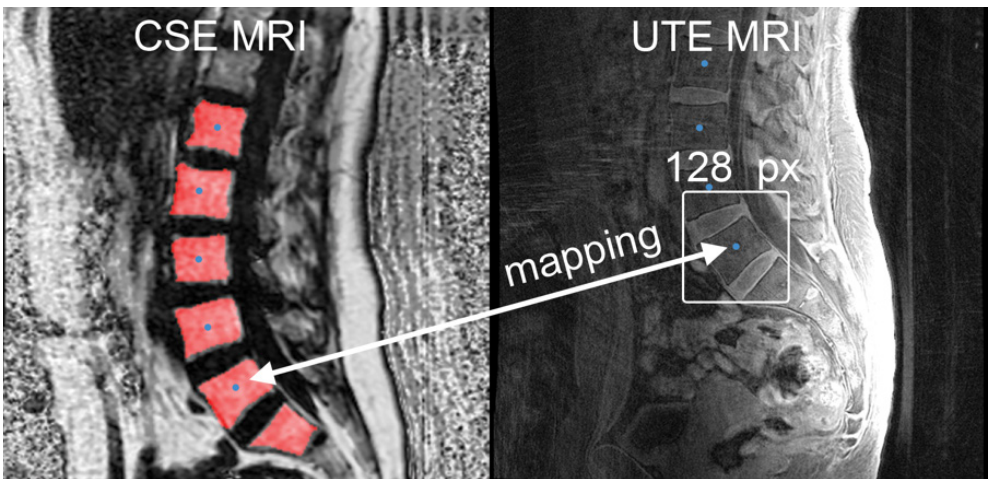

Figure S1 Lumbar vertebral segmentations (red) for the CSE images were used to identify the L5 vertebral body centroid in CSE and UTE space to facilitate automated image cropping. CSE, chemical-shift encoding based; UTE, ultra-short echo time; MRI, magnetic resonance imaging.

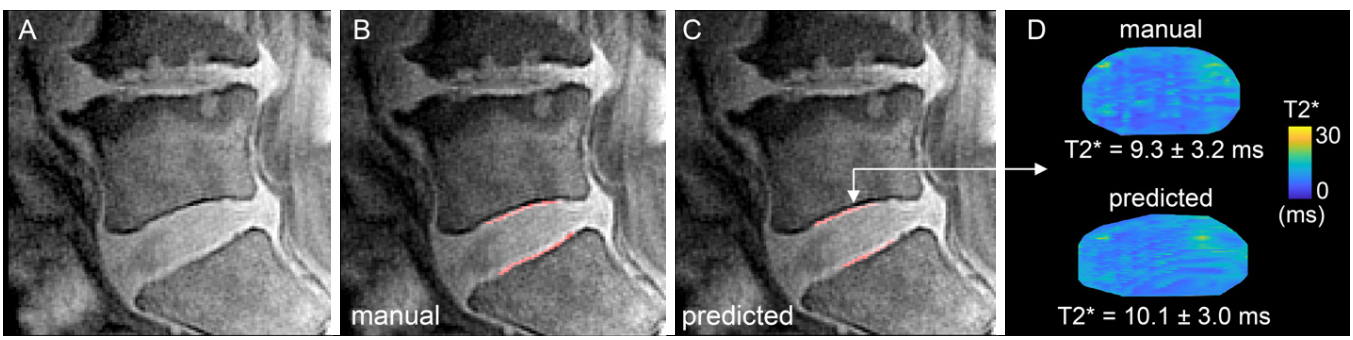

Figure S2 (A) Mid-sagittal UTE image collected using a second scanner showing endplate damage at L4-L5. This level was excluded from analysis. (B) Manually- and (C) model-generated CEP segmentations (red) at L5-S1. (D) Transverse T2* maps generated from these segmentations show a similar distribution and mean ± SD T2* values in the central CEP. UTE, ultra-short echo time; CEP, cartilage endplate; SD, standard deviation.

https://dx.doi.org/10.21037/qims-22-729